

THE CIRCUMSTELLAR SHELL OF THE POST-ASYMPTOTIC GIANT BRANCH STAR HD 56126: THE $^{12}\text{CN}/^{13}\text{CN}$ ISOTOPE RATIO AND FRACTIONATION

ERIC J. BAKKER¹ AND DAVID L. LAMBERT

Department of Astronomy and W. J. McDonald Observatory, University of Texas, Austin, TX 78712-1083; ebakker@astro.as.utexas.edu, dll@astro.as.utexas.edu

Received 1997 August 5; accepted 1998 February 25

ABSTRACT

We have detected circumstellar absorption lines of the ^{12}CN and ^{13}CN violet and red system in the spectrum of the post-AGB star HD 56126. From a synthetic spectrum analysis, we derive a Doppler broadening parameter of $b = 0.51 \pm 0.04 \text{ km s}^{-1}$, $^{12}\text{CN}/^{13}\text{CN} = 38 \pm 2$, and a lower limit of 2000 on $^{12}\text{CN}/^{14}\text{CN}$ and $^{12}\text{C}^{14}\text{N}/^{12}\text{C}^{15}\text{N}$. A simple chemical model has been computed of the circumstellar shell surrounding HD 56126 that takes into account the gas-phase ion-molecule reaction between CN and C^+ . From this we infer that this reaction leads to isotopic fractionation of CN. Taking into account the isotopic exchange reaction and the observed $^{12}\text{CN}/^{13}\text{CN}$, we find $^{12}\text{C}/^{13}\text{C} \sim 67$ (for $T_{\text{kin}} = 25 \text{ K}$). Our analysis suggests that ^{12}CN has a somewhat higher rotational temperature than ^{13}CN : $T_{\text{rot}} = 11.5 \pm 0.6$ and $8.0 \pm 0.6 \text{ K}$, respectively. We identify possible causes for this difference in excitation temperature, among which is the N'' dependence of the isotopic exchange reaction.

Subject heading: line: identification — molecular data — molecular processes — stars: AGB and post-AGB — stars: circumstellar matter — stars: individual (HD 56126)

1. INTRODUCTION

The evolution of a low-mass red giant terminates on the tip of the asymptotic giant branch (AGB). The remnant, a carbon-oxygen core with a dilute extended convective envelope, evolves along a constant luminosity track toward the white dwarf (WD) phase. This transition from AGB to WD is referred to as the post-AGB phase, or the pre-planetary nebulae (PPN) phase. Since low-mass stars are the main contributors of carbon, nitrogen, and *s*-process elements to the interstellar medium (ISM) (Forestini & Charbonnel 1997), accurate information on the chemical composition of AGB and post-AGB stars is important. Post-AGB stars may provide useful information as to the composition of the gas returned to the ISM. In particular, the fact that their spectra are much simpler than those of the cool AGB stars affords novel opportunities for inferring details of the composition of AGB stellar envelopes.

The present photosphere of HD 56126 ($T_{\text{eff}} = 7000 \text{ K}$) is carbon-rich ($\text{C}/\text{O} \simeq 1.4$), metal-poor ($[\text{Fe}/\text{H}] \simeq -1.0$), and enhanced in *s*-process elements ($[\text{s}/\text{Fe}] = 1.7$) (Klochkova 1995). Such an abundance pattern resembles that of carbon stars (Lambert et al. 1986; Utsumi 1970), resulting from the dredge-up of nucleosynthesis products as the star evolves up the AGB. HD 56126 is the prototype of a group of post-AGB and AGB stars that exhibit absorption lines from circumstellar C_2 and CN (from this point, C will mean ^{12}C and N will mean ^{15}N) in their spectra (Bakker et al. 1996, hereafter Paper I; Bakker et al. 1997, hereafter Paper II). In order to facilitate further discussion, we introduce the term “C2CN stars” to refer to this group of stars. Molecules are present in the detached shell surrounding the star, and the chemical composition of the dusty shell reflects the photospheric composition of the star when it was at the tip of the AGB (TP-AGB). The molecular composition of the shell has evolved; for example, a simple molecule such as CN is

believed to be formed as a result of photodissociation of complex molecules (in this case HCN) by the interstellar radiation field.

Excitation of the CN molecule’s $X^2\Sigma^+$ ground state is likely to be controlled by absorption and reemission of photons in the violet ($B^2\Sigma^+ \rightarrow X^2\Sigma^+$) and red ($A^2\Pi \rightarrow X^2\Sigma^+$) system, and pure rotational transitions (principally deexcitation) in the $X^2\Sigma^+$ state. At the low densities of the circumstellar shell, the pure rotational transitions will cool the rotational ladder below the gas kinetic temperature (subthermal). For a symmetric molecule without a dipole moment (e.g., C_2), pure rotational transitions are forbidden and the molecule can not efficiently cool. The excitation temperature is higher than the kinetic temperature of the gas (suprathermal). Through measurement of the level population and modeling of the (de)excitation processes, the CN molecule serves as a probe of the physical conditions in the shell. A molecule such as CN also affords us an opportunity to compare column densities of isotopomers, e.g., the ratio of CN to ^{13}CN . In turn, understanding the chemistry allows us to derive the isotopic ratio $^{12}\text{C}/^{13}\text{C}$ from the measured $^{12}\text{CN}/^{13}\text{CN}$ ratio.

In this paper (Paper III), we present and discuss the first measurement of the CN/ ^{13}CN ratio and an estimate of the $^{12}\text{C}/^{13}\text{C}$ ratio and lower limits on $^{12}\text{C}/^{14}\text{C}$ and $^{14}\text{N}/^{15}\text{N}$ in the circumstellar shell of a post-AGB star. In § 2 we discuss the observations and the data set of equivalent widths used in our analysis. Section 3 goes into the details of the molecular parameters used, and § 4 describes the analysis and results. A discussion of the results is presented in § 5.

2. OBSERVATIONS AND EQUIVALENT WIDTHS

High-resolution spectra were obtained with the 2.7 m Harlan J. Smith telescope of the W. J. McDonald observatory and the coudé cross-dispersed echelle spectrograph (Tull et al. 1995). We acquired spectra of the $(v' - v'') = (0-0)$ band of the CN violet system at a resolution of $R = \lambda/\Delta\lambda \simeq 140,000$, and spectra of the (3-0) and (4-0) bands of the CN red system at $R \simeq 200,000$. Observations

¹ Current address: TNO-FEL, Electro Optics Group, P.O. Box 96864, 2509 JG The Hague, The Netherlands; e.j.bakker@fel.tno.nl.

TABLE 1
LOG OF OBSERVATIONS

Observation Parameter	HJD	Interval (s)	$R = \lambda/\Delta\lambda$	λ_c (Å)	S/N	Remarks
Date						
1996 Dec 29	2450446.7158	6×1800	200,000	7558	100	Red (3, 0) + H α
1997 Jan 02	2450450.8708	3×1800	140,000	4062	20	Violet (0, 0) + Ca II H + He
1997 Feb 28	2450507.5840	6×1800	140,000	4056	15	Violet (0, 0) + H δ
1997 Mar 01	2450508.5696	6×1800	140,000	3874	22	Violet (0, 0) + H δ
1997 Mar 03	2450510.6087	8×1800	200,000	6086	70	Red (3, 0) + Red (4, 0)
Coadded spectra						
Violet system (0, 0).....		7.5 hr	140,000	3877	35	
Red system (3, 0).....		7.0 hr	200,000	6945	200	
Red system (4, 0).....		4.0 hr	200,000	6195	90	

were made from 1996 December to 1997 March (Table 1). The spectral resolution of the spectra were determined from the FWHM of the emission lines in the accompanying ThAr arc spectrum and corrected for the intrinsic width of the ThAr emission lines.

Observations of 30 minutes have been coadded to give the final spectra for each night. All spectra were reduced using IRAF in the standard manner. Individual integrations were corrected for the velocity shift due to the Earth's rotation and instrumental drift before combining them to an average spectrum. The final S/N ratio of the spectra is 35 for the violet (0–0) band and 200 and 90 for the red (3–0) and (4–0) bands, respectively.

Portions of the final spectra are shown in Figures 1 and 2. From each final spectrum, we removed the molecular features and fitted a high-order spline that followed all photospheric features. The observed spectrum was divided by this fit to obtain the rectified spectrum, which only contains the molecular features. Circumstellar CN lines are readily dis-

tinguishable from the much broader photospheric lines of various atomic species. The equivalent widths (Tables 2 and 3) of the molecular lines were measured relative to the local continuum (taking into account stellar absorption lines). A search for ^{14}CN and C^{15}N in the violet system (0, 0) band was unsuccessful; an upper limit to their equivalent width is 1.5 mÅ.

HD 56126 is a pulsating star. The photospheric spectrum from the star therefore might change from one run to the next, and combining the spectra from different runs could lead to errors. We have therefore measured the equivalent width of the lines for each night separately and averaged to obtain the final equivalent width. The spectra in Figures 1 and 2 are combined using all available data, and there is no indication that the photospheric spectrum has indeed changed from one run to the next.

This high-quality data set was extended with previous data for the red system (1, 0), (2, 0), and (3, 0) bands (presented in Paper I), provided by spectra collected with

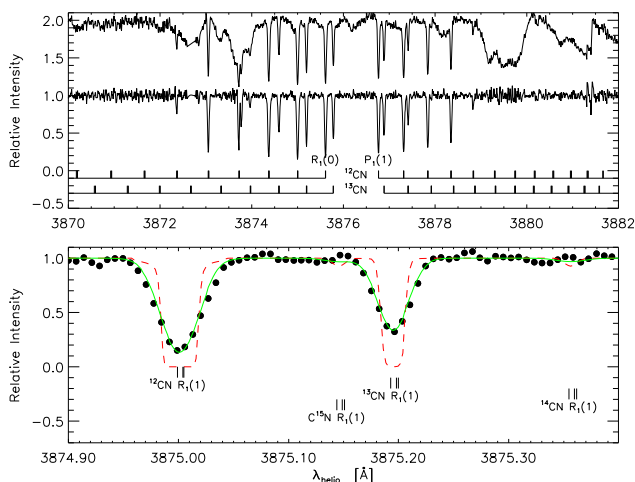


FIG. 1.—CN violet system (0, 0) band toward HD 56126. Upper panel shows the observed spectrum and a rectified spectrum corrected for the underlying photospheric features. The rectified spectrum contains only circumstellar lines. Lower panel shows, on an expanded wavelength scale, the strongest line (the R_1 , R_2 , and ${}^R Q_{2,1}$ blend for $N'' = 1$), and demonstrates that we have not detected ^{14}CN and C^{15}N . The dashed spectrum line shows a synthetic spectrum computed for $b = 0.51 \text{ km s}^{-1}$, $T_{\text{rot}} = 11.5 \text{ K}$ for CN, $T_{\text{rot}} = 8.0 \text{ K}$ for the CN isotopes, and the isotope or lower-limit isotope ratios as determined in this work. The solid spectrum line shows the synthetic spectrum convolved to our spectral resolution of $R = 140,000$.

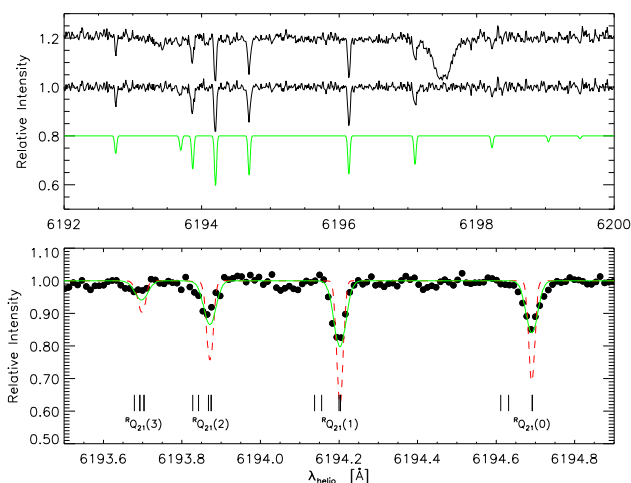


FIG. 2.—CN red-system (4, 0) band toward HD 56126. Upper panel shows the observed spectrum (offset by 0.2), a rectified spectrum corrected for the underlying photospheric features, and a convolved synthetic spectrum (offset by -0.2). The rectified spectrum contains only circumstellar lines. Lower panel shows an expanded wavelength scale centered around the strongest line [the ${}^R Q_{2,1}(1)$ or $R_2(1)$ blend]. Dashed and solid synthetic spectrum lines are as in Fig. 1. The ^{13}CN (4, 0) band is redshifted by about 54 Å, and so not covered by this spectrum. The solid spectrum line shows the synthetic spectrum convolved to our spectral resolution of $R = 200,000$.

TABLE 2
CN VIOLET SYSTEM (0, 0) WITH $f_{(0,0)} = 0.0330$

$B(N'')$	λ_{rest} (Å) CN ^b	$\Delta\lambda^a$ (Å)			$f_{N'J',N''J''}$	$f_{\text{eff}} N$ (cm ⁻²)	W_λ (mÅ)		REMARKS
		¹³ CN ^b	¹⁴ CN ^b	C ¹⁵ N ^b			CN	¹³ CN	
$R_1(6)$	3870.6661	0.3481	0.604c	0.239c	0.0176	0.0178N(6)	<2.0	<2.0	
$R_2(6)$	3870.6571				0.0178				
${}^R Q_{21}(6)$	3870.665c				0.0002				
$R_1(5)$	3871.3581	0.3001	0.550c	0.218c	0.0178	0.0180N(5)	9.6 ± 0.3	<2.0	
$R_2(5)$	3871.3661				0.0180				
${}^R Q_{21}(5)$	3871.371c				0.0002				
$R_1(4)$	3872.0451	0.2771	0.497c	0.197c	0.0180	0.0183N(4)	29.0 ± 0.5	<1.7	too strong
$R_2(4)$	3872.0531				0.0183				
${}^R Q_{21}(4)$	3872.058c				0.0003				
$R_1(3)$	3872.7161	0.2521	0.446c	0.176c	0.0183	0.0189N(3)	25.1 ± 0.3	6.3 ± 0.5	perturbed
$R_2(3)$	3872.7121				0.0189				
${}^R Q_{21}(3)$	3872.725c				0.0006				
	3872.7741						10.0 ± 0.3		perturbation
$R_1(2)$	3873.3631	0.2221	0.396c	0.156c	0.0189	0.0198N(2)	37.1 ± 0.3	18.6 ± 0.3	
$R_2(2)$	3873.3701				0.0198				
${}^R Q_{21}(2)$	3873.3711				0.0009				
$R_1(1)$	3873.9911	0.1921	0.348c	0.137c	0.0198	0.0220N(1)	36.7 ± 0.3	25.0 ± 0.3	
$R_2(1)$	3873.9961				0.0220				
${}^R Q_{21}(1)$	3873.9981				0.0022				
$R_1(0)$	3874.6021	0.1761	0.301c	0.119c	0.0220	0.0330N(0)	36.3 ± 0.3	21.1 ± 0.4	
${}^R Q_{21}(0)$	3874.6051				0.0110				
${}^P Q_{12}(1)$	3875.7581				0.0110				
$P_1(1)$	3875.7591	0.130o	0.212c	0.083c	0.0110	0.0110N(1)	32.6 ± 0.3	18.4 ± 0.3	
${}^P Q_{12}(2)$	3876.3041				0.0022				
$P_1(2)$	3876.3061	0.1051	0.170c	0.067c	0.0132	0.0132N(2)	29.0 ± 0.3	13.7 ± 0.3	
$P_2(2)$	3876.3081				0.0110				
${}^P Q_{12}(3)$	3876.830c				0.0009				
$P_1(3)$	3876.8341	0.0631	0.130c	0.050c	0.0141	0.0141N(3)	27.6 ± 0.3	4.2 ± 0.5	
$P_2(3)$	3876.8361				0.0132				
${}^P Q_{12}(4)$	3877.336c				0.0006				
$P_1(4)$	3877.3411	0.0561	0.091c	0.035c	0.0147	0.0147N(4)	24.1 ± 0.3	<1.0	
$P_2(4)$	3877.3451				0.0141				
${}^P Q_{12}(5)$	3877.821c				0.0003				
$P_1(5)$	3877.8281	0.028c	0.054c	0.020c	0.0150	0.0150N(5)	3.9 ± 0.5	polluted	perturbed
$P_2(5)$	3877.8251				0.0147				
	3877.8851						<1.0		perturbation
${}^P Q_{12}(6)$	3878.286c				0.0002				
$P_1(6)$	3878.2941	0.008c	0.018c	0.006c	0.0152	0.0152N(6)	<1.0	<1.0	
$P_2(6)$	3878.3001				0.0150				

NOTE.—Derived column densities are given in Table 4.

^a Isotopic shift relative to CN. Example: $R_2(1)$ ¹⁴CN at $3873.996 + 0.348 = 3874.344$ Å.

^b c: computed; l: laboratory data; o: spectrum. For lines with laboratory data, $v(\text{CN}) = 77.5 \pm 0.5$ km s⁻¹ and $v(^{13}\text{CN}) = 76.7 \pm 1.8$ km s⁻¹.

the WHT/UES at a spectral resolution of $R \approx 50,000$. Our new measurements for the red (3–0) band are in good agreement with the measurements of Paper I. The weaker lines were only detected at our higher resolution.

3. MOLECULAR DATA

3.1. CN Violet System

Wavelengths for the CN violet system (0, 0) were computed from the wavenumbers of Prasad et al. (1992), and the

isotopic wavelengths for the ¹³CN violet system (0, 0) were computed from Jenkins & Wooldridge (1938). The isotopic shift of the ¹³CN P_1 ($N'' = 1$) blend was obtained from our observed spectrum. Line positions not listed in these papers were computed using the molecular constants given by Prasad et al. (1992) and the standard relations for the mass dependence of the various molecular constants (cf. Bernath 1995). The computed wavenumbers were in good agreement with the laboratory measurements. Predictions were

TABLE 3
CN RED SYSTEM (4, 0) WITH $f_{(4,0)} = 1.09 \times 10^{-4}$

$B(N'')$	λ_{rest}^a (Å)	$f_{N'J',N''J''}$ ($\times 10^4$)	$f_{\text{eff}} \times 10^4 N(N'')$ (cm^{-2})	W_λ (mÅ)
$^S R_{21}(3)$	6186.2931	0.101	0.058N(3)	≤ 1.5
$^S R_{21}(2)$	6187.7641	0.112	0.067N(2)	1.8 ± 0.5
$^S R_{21}(1)$	6189.3971	0.127	0.085N(1)	3.1 ± 0.5
$^S R_{21}(0)$	6191.159c	0.151	0.151N(0)	2.4 ± 0.1
$R_2(3)$	6192.0871	0.202		
$^R Q_{21}(3)$	6192.101c	0.217	0.211N(3)	≤ 1.5
$R_2(2)$	6192.2551	0.203		
$^R Q_{21}(2)$	6192.274c	0.237	0.223N(2)	5.3 ± 0.6
$R_2(1)$	6192.572c	0.215		
$^R Q_{21}(1)$	6192.6051	0.264	0.248N(1)	8.0 ± 0.2
$^R Q_{21}(0)$	6193.0081	0.363	0.363N(0)	7.2 ± 0.1
$Q_2(1)$	6194.4851	0.363	0.182N(1)	6.7 ± 0.1
$^Q P_{21}(1)$	6194.550c	0.091		
$Q_2(2)$	6195.4671	0.316	0.188N(2)	4.5 ± 0.5
$^Q P_{21}(2)$	6195.515c	0.102		
$Q_2(3)$	6196.6221	0.323	0.197N(3)	1.7 ± 0.2
$^Q P_{21}(3)$	6196.638c	0.103		
$P_2(2)$	6197.4581	0.091	0.036N(2)	≤ 1.5

NOTE.—Derived column densities are given in Table 4.

^a c: computed; l: laboratory data; o: spectrum. For lines with laboratory data, $v(\text{CN}) = 77.5 \pm 0.5 \text{ km s}^{-1}$ and $v(^{13}\text{CN}) = 76.7 \pm 1.8 \text{ km s}^{-1}$.

extended to the isotopes ^{14}CN and C^{15}N . Table 2 lists the wavelength shift of the various isotopes relative to CN. The isotopic shift is the same for the three lines within one blend; for example, the $^{13}\text{CN } ^R Q_{21}(2)$ line is at 3873.593 \AA . In all cases, the index of refraction of standard air was computed using the formula given by Morton (1991).

The f_V -value of the violet system is well determined experimentally and theoretically. Theoretical calculations by Knowles et al. (1988) and Bauschlicher, Langhoff, & Taylor (1988) predict $f_V(0-0) = 0.0345$ and 0.0335 , respectively. An earlier calculation by Larsson, Siegbahn, & Ågren (1983) gave $f_V(0-0) = 0.0324$. The most accurate experimental results are the measurements of the radiative lifetime of the $B^2\Sigma^+$ state. Low rotational states of the $v' = 0$ level of the B state have measured lifetimes (in ns) of 60.8 ± 2.0 (Luk & Bersohn 1973), 65.1 ± 0.8 (Jackson 1974), and 66.7 ± 1.4 (Duric, Erman, & Larsson 1978). Theoretical values (including the small contribution from $B^2\Sigma^+ \rightarrow A^2\Pi$) are 60.7 (Knowles et al. 1988), 62.4 (Bauschlicher et al. 1988), and 66.6 (Larsson et al. 1983). We adopt $f_V(0-0) = 0.033$, which is approximately the average of these various theoretical and experimental estimates. The uncertainty is not more than a few percent.

3.2. CN Red System

Accurate wavelengths of red-system CN lines were taken from Davis & Phillips (1963), and the isotopic shifts for the ^{13}CN red system were taken from Hosinsky, Klyning, & Lindgren (1981). Wavelengths not found in the literature were computed using the molecular constants of Prasad &

Bernath (1992) and compared to those of the SCAN tape (Jørgensen & Larsson 1990).

Theory and experiment have not yet fully converged for the red system f_R -value (see the brief review by Larsson 1994). Theoretical predictions are $f_R(3-0) = 3.34 \times 10^{-4}$ (Knowles et al. 1988), 3.35×10^{-4} (Bauschlicher et al. 1988), and 4.58×10^{-4} (Larsson et al. 1983). Davis et al. (1986) measured the f_R -values of six red-system bands relative to the violet (0-0) band using absorption lines produced by the transmission of light through a column of CN in a furnace. Their result, adjusted by 3% to account for the difference between their adopted value and the above recommendation for $f_V(0-0)$, gives $f_R(3-0) = (2.9 \pm 0.2) \times 10^{-4}$, a value slightly smaller than the most recent theoretical calculations. The results of Davis et al. (1986) for other bands were similarly smaller than the theoretical predictions. Gredel, van Dishoeck, & Black (1991) analyze observations of CN violet (0-0) and red (2-0) interstellar absorption lines in the same line of sight using the f -values $f_V(0-0) = 0.0342$ and $f_R(2-0)$ from Davis et al. (1986). Gredel et al. (1991) remark that the violet and red lines give the same column density, but “a slightly higher red-system oscillator strength would improve the agreement between the violet and the red system data.” Inspection of the results of Gredel et al. (1991) suggests that the theoretical values given by Knowles et al. (1988) and Bauschlicher et al. (1988) fit the suggestion of “a slightly higher” f_R -value, but the value found by Larsson et al. (1983) is probably too large. There remains an unresolved question posed by measurements of the radiative lifetimes of vibrational levels of the $A^2\Pi$ state. What appear to be the best measurements, radiative lifetimes from laser-induced fluorescence (Lu, Huang, & Halpern 1992), are consistently shorter than the theoretical predictions; the difference amounts to about 30% for $v' = 0$, but is a factor 3 for $v' = 7$. These lifetimes imply that our adopted f_R -values may be underestimates. We adopt the f_R -value given by Knowles et al. (1988) and Bauschlicher et al. (1988), with a small correction for our adopted f_V value: $f_R(0-0) = 23.7 \times 10^{-4}$, $f_R(1-0) = 19.1 \times 10^{-4}$, $f_R(2-0) = 9.0 \times 10^{-4}$, $f_R(3-0) = 3.3 \times 10^{-4}$, and $f_R(4-0) = 1.1 \times 10^{-4}$.

3.3. Oscillator Strength of Individual Lines

The oscillator strength of a transition is given to an acceptable precision by $f_{N'J',N''J''} = (v_{N'J',N''J''}/v_0) f_{v'v''} S_{J'J''}/(2J'' + 1)$, where $v_{N'J',N''J''}$ and v_0 are the frequency of the transition and the band origin, respectively. The parameter $f_{v'v''}$ is the band oscillator strength discussed in §§ 3.1 and 3.2, and $S_{J'J''}$ is the Hönl-London factor (also called the natural line strength). The computation of the Hönl-London factors is described in the Appendix.

Almost all CN “lines” consist of two or three unresolved transitions. For example, the R-branch lines of the violet system (Table 2 and Fig. 1) are effectively a triplet of transitions [$R_1(N'')$, $R_2(N'')$, and $^R Q_{21}(N'')$]. For the red system, several branches provide an accompanying satellite line (Table 3 and Fig. 2), e.g., $R_2(N'')$ is accompanied by $^R Q_{21}(N'')$.

The determination of column densities may use a curve of growth computed for a single line. If unresolved components of a blend are separated by more than about the Doppler width, $\Delta\lambda_D$, the equivalent width of the lines of individual transitions are added. If the separation is much less than $\Delta\lambda_D$, the blend may be presented as a single line with a so-called effective oscillator strength (see Appendix).

For separations comparable to $\Delta\lambda_D$, there is no simple way to represent the blend on the curve of growth for a single line.

A correct treatment of the overlap of spectral lines in a blend necessarily requires the computation of synthetic spectra. A computer program (MOLLEY-CN) was developed that computes wavenumbers, Hönl-London factors, and oscillator strength for any (isotopic) band of the CN red and violet system. From these numbers, a synthetic spectrum based on a Voigt profile is computed. Inputs to the program are the rotational temperature, total column density, isotope ratios, Doppler b -parameter, and the spectral resolution of the output spectrum. (MOLLEY-CN is available on request from the authors.) As an aid to those who prefer the method of effective oscillator strength, we have investigated the error that this method introduces into the derived column densities. For this purpose, we have chosen the CN violet (0, 0) $R(2)$ blend, for which the two principal transitions are separated by 0.54 km s^{-1} . For a range of Doppler b -parameters, the column density of the $N'' = 2$ (F_1 and F_2) level has been computed using the effective oscillator strength and synthetic spectra for a line with an equivalent width of $37.1 \text{ m}\text{\AA}$. Figure 3 demonstrates the results. The derived b -parameter in this work is $b = 0.51 \pm 0.04 \text{ km s}^{-1}$, and the effective oscillator strength method is clearly unacceptable here. We therefore will use the method of computing synthetic spectra to determine the column density responsible for the observed equivalent width of a blend. The only remaining limitation is that the line might be blended with transitions originating from other N'' levels, and that the rotational temperature must be given to compute such a blend. This limitation is easily overcome by iteration, using an improved estimate of the rotational temperature.

Figure 3 can be qualitatively understood in the following way. Using f_{eff} assumes that the lines that form a blend [$R(2)$ is a triplet] have exactly the same wavelength. This approximation is valid only for b -values much larger than the separation between the lines of a blend. Figure 3 demonstrates this, since the computed column densities from the two methods are the same for large b -values. For small

b -values, the use of f_{eff} fails because the lines are (partly) separated and the blend absorbs more efficiently than assumed by the f_{eff} method. For a given equivalent width of a line, this means that the spectrum synthesis method yields a lower column density than the f_{eff} method. The $R(2)$ blend has three lines. For moderate column densities, the contribution of the weakest line [${}^R Q_{2,1}(2)$] can be neglected and the ratio of the column density as derived from the two-line method is given by the inverse of the slope of the curve of growth. The slope is 1 for the linear part, 0.5 for the damping wings, and < 0.5 for the saturated part of the curve of growth, and the maximum ratios are therefore 1, 2, and > 2 . We see in Figure 3 that the ratio goes to 2 when the two strongest lines of the triplet are on the saturated part of the curve of growth. For larger column densities, the blend is highly saturated and the broad damping wings contribute significantly to the equivalent width. The damping wings will be the same in both cases and the ratio will go to 1. We note that in the real world, lines never become this strong.

4. ANALYSIS

4.1. Velocities

From the molecular lines with tabulated laboratory wavenumbers, we find an average heliocentric radial velocity of $77.5 \pm 0.5 \text{ km s}^{-1}$. To within the errors of the measurements, the velocity is independent of the rotational level N'' . All velocities given in this article are corrected to the heliocentric rest frame. HD 56126 is a pulsating star (Oudmaijer & Bakker 1994; Lèbre et al. 1996; Paper II), and the photospheric velocity derived from our spectra will not be a good estimate of the systemic velocity of the star. In order to derive an expansion velocity, we use the systemic velocity derived from CO radio line emission (for an overview, see Paper I). For $v_{*,\text{CO}} = 85.6 \pm 0.5 \text{ km s}^{-1}$, we arrive at an expansion velocity of $v_{\text{exp}} = 8.1 \pm 0.7 \text{ km s}^{-1}$. This result is consistent with that derived from the width of the CO lines, $v_{\text{exp}} = 12.1 \pm 1.0 \text{ km s}^{-1}$ (Nyman et al. 1992). The expansion velocity is similar to expansion velocities of AGB stars, suggesting that the molecule-containing layer around the post-AGB star, which is possibly part of the terminal “superwind” of the AGB star, was not ejected at very high velocity (Fig. 3).

4.2. Doppler b -Parameter and Synthetic Spectra

In Paper I it was demonstrated that the red-system (3, 0) band is just saturated, while the stronger (2, 0) and (1, 0) are saturated. From this it is obvious that the violet system (0–0) band with f_v -values a factor of 10 higher than the red system must be highly saturated. Of course, this circumstance facilitates detection of the ${}^{13}\text{CN}$ lines. The degree of saturation can be judged from Figure 4, which shows curves of growth for each N'' level. Observed lines from a given N'' level are combined into a single curve using the adopted f -values. The fitted theoretical curve is computed from a single line, assuming $b = 0.51 \text{ km s}^{-1}$. Clearly, the unsaturated lines are all from the red system, 3–0 and 4–0 for the $N'' = 0$ level, but extending to the 1–0 band for the $N'' = 3$ level. For all relevant N'' levels, the ${}^{12}\text{CN}/{}^{13}\text{CN}$ ratio is obtainable from a comparison of ${}^{13}\text{CN}$ violet system lines with CN red-system lines of about the same strength. Thus, the ${}^{12}\text{CN}/{}^{13}\text{CN}$ ratio is insensitive to the b -value, but dependent on the ratio of the f -values for the violet and red systems. A sensitivity to the b -value does exist because, as

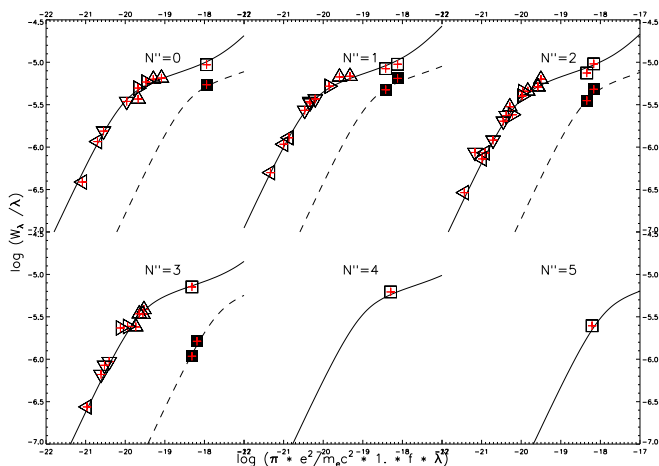


FIG. 3.—Curve of growth for each N'' level. The displacement of CN (solid line) and ${}^{13}\text{CN}$ (dashed line) along the horizontal axis give the isotope ratio derived from that N'' level. Squares show the violet system (0, 0), and triangles show the red-system bands [triangle pointing up, (1, 0); right, (2, 0); down, (3, 0); and left, (4, 0)]. The overplotted theoretical model is for $b = 0.51 \text{ km s}^{-1}$.

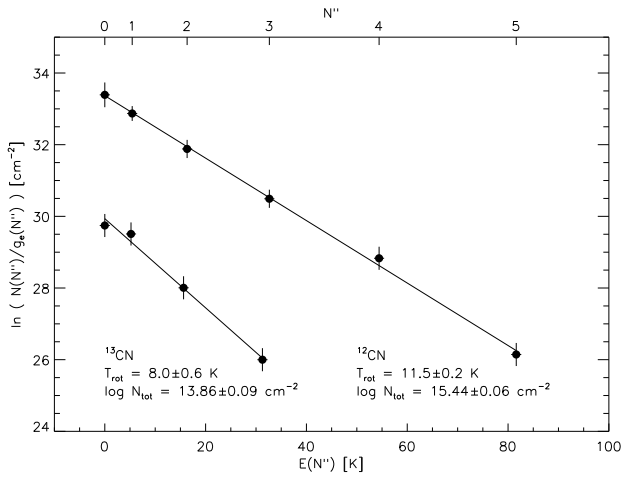


FIG. 4.—Rotational diagram for CN and ^{13}CN with the column densities of Table 4 ($b = 0.51 \text{ km s}^{-1}$). Note that the slope of the two curves are different. This translates into CN having a higher rotational temperature than ^{13}CN .

noted above, the precise curve of growth is dependent on the makeup of individual CN features. For a detailed analysis, we must determine the Doppler b -parameter and derive column densities from the observed equivalent widths by taking into account the details of the blends and optical depth effects.

For each transition (spectral line), there are two unknown parameters that affect the observed equivalent width: the Doppler b -parameter and the column density of the level from which the transition originates [$N(N'')$]. The b -parameter must be the same for all lines, under the assumption that they are all formed from the same gas. The $N(N'')$ is the same for transitions for a given level N'' of the same isotope. In this study we included $N'' = 0, 1, 2, 3, 4,$ and 5 for CN and $N'' = 0, 1, 2,$ and 3 for ^{13}CN ; thus, ten independent column densities. We assumed that the F_1 and F_2 level populations are given by their degeneracy level and the energy of the average N'' level. We solved for b and $N(N'')$ in the following manner.

For a range of b -parameters ($0.10 \leq b \leq 2.60 \text{ km s}^{-1}$ in steps of 0.01 km s^{-1}), the column density responsible for the observed equivalent width of the blend is determined by

means of spectrum synthesis. We did not fit the observed spectra directly, but instead used the observed equivalent width. Although we have ten independent measurements of the b -parameter, most of the N'' levels are only probed by one or two lines, and the errors are rather large. We have therefore limited the analysis to the CN $N'' = 0, 1, 2,$ and 3 levels, which are each probed by at least ten blends. For each b -parameter, $\log N(N'')$ and its standard deviation where computed. The final b -parameter is given by the combination for which the standard deviation is minimal, and by averaging the b -parameter weighted by the number of lines. The CN Doppler parameter was found to be $b = 0.51 \pm 0.04 \text{ km s}^{-1}$. This same process was repeated for C_2 using the data of Paper I, resulting in $b = 0.53 \pm 0.03 \text{ km s}^{-1}$. Since the CN data is of higher quality, we adopt $b = 0.51 \pm 0.04 \text{ km s}^{-1}$ for both CN and C_2 . Given the b value, the FWHM of the absorption line profile should be at least $0.85 \pm 0.05 \text{ km s}^{-1}$. In order to resolve these lines, a spectral resolution of $R \geq 350,000$ is needed. This confirms that we are not able to resolve these line profiles in our spectra. The line profiles of the synthetic spectra can be perfectly fitted to the observed ones for this b -value convolved to the spectral resolution of the observations. No additional macroturbulent broadening is needed to explain the observations.

4.3. Column Densities and Rotational Temperatures

Some additional lines were observed that are identified as due to perturbations (Prasad et al. 1992). Perturbations occur from the crossing of energy levels in two different electronic manifolds (Kotlar, Field, & Steinfeld 1980). The perturbations in the violet system (0, 0) band originate from $B^2\Sigma v = 0$ levels perturbed by the $A^2\Pi v = 10$ level. Perturbations affect the oscillator strength of lines. Since a study of the perturbations is beyond the scope of this work, we will not include the perturbed lines in our analysis.

The derived average column density per N'' level and isotope are listed in Table 4. Given these column densities, an absolute rotational diagram can be constructed (Fig. 5) and the rotational temperature can be determined. Using a first-order fit (constant T_{rot}), we find $T_{\text{rot}}(\text{CN}) = 12.8 \pm 0.6 \text{ K}$, and $T_{\text{rot}}(^{13}\text{CN}) = 8.0 \pm 0.6 \text{ K}$. The rotational temperature for $N'' = 0, 1, 2,$ and 3 of CN is determined very largely by the weak CN red system lines, especially the (3–0)

TABLE 4
COLUMN DENSITIES AND THE ISOTOPE RATIOS DERIVED FROM SPECTRUM SYNTHESIS FOR $b = 0.51 \text{ km s}^{-1}$ AND THE f -VALUES GIVEN IN §§ 3.1 AND 3.2.

N''	log $N(N'')$						
	CN ^{a,b}	^{13}CN ^{a,b}	^{14}CN	C^{15}N	CN/ ^{13}CN ^b	CN/ ^{14}CN	CN/ ^{15}CN
0.....	14.80 ± 0.17(10)	13.22 ± 0.10(1)			38.3 ± 3.0		
1.....	15.05 ± 0.17(12)	13.59 ± 0.10(2)	≤11.72	≤11.72	28.8 ± 2.1	≥2000	≥2000
2.....	14.85 ± 0.16(17)	13.16 ± 0.10(2)			48.2 ± 2.8		
3.....	14.39 ± 0.13(11)	12.44 ± 0.10(2)			89.2 ± 3.9		
4.....	13.78 ± 0.10(01)	≤11.79					
5.....	12.70 ± 0.10(01)						
6.....	≤11.79						
Total.....	15.44 ± 0.06(52)	13.86 ± 0.09(7)	≤11.72	≤11.72	38.0 ± 1.5 ^c	≥2000 ^c	≥2000 ^c
T_{rot} (K).....	11.5 ± 0.2	8.0 ± 0.6					

NOTE—

^a Numbers in parentheses give the number of lines used to determine the average column density.

^b Errors are the standard deviations on the average; if less than 4 lines, 0.10 was adopted.

^c Preferred ratios.

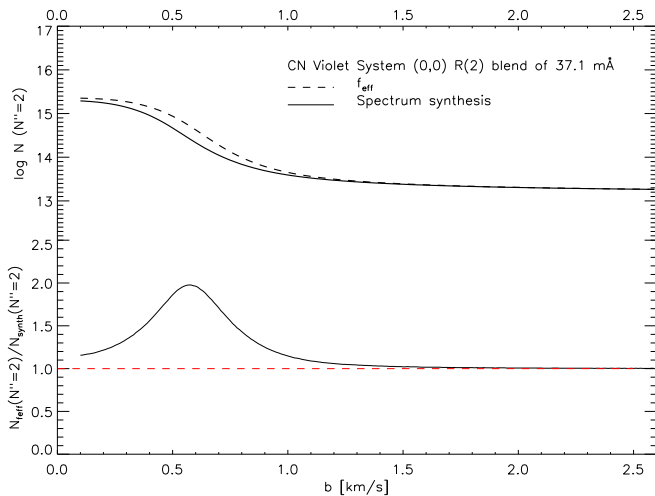


FIG. 5.—Comparison of the derived column density of the $N'' = 2$ level from the CN violet system (0, 0) $R(2)$ line at 3873.37 Å. The solid line is obtained from the spectrum synthesis method, while the dashed line uses the effective oscillator strength and a curve of growth for a single, unblended line. The separation between the two principal lines of the blend is 0.54 km s^{-1} .

and (4–0) lines measured off our McDonald spectra: $T_{\text{rot}}(\text{CN}) = 11.1 \pm 0.8 \text{ K}$. For $N'' = 4$ and 5, the column density is set almost exclusively by a CN violet system line that, in the case of $N'' = 4$, is partially saturated; the $N'' = 4$ and 5 levels give a temperature of $T_{\text{rot}}(\text{CN}) = 10.8 \pm 0.8 \text{ K}$ that within the errors is identical to the temperature from $N'' = 0$ to 3. The column density for $N'' = 4$ and 5 seems higher by 0.3 dex than given by extrapolation from $N'' = 0$ to 3. This offset, corresponding to a reduction of the red-system f_R -values by a factor of 2 (relative to the violet system), is probably excluded by experimental and theoretical results for the f -values (see above). A single rotational temperature (Table 4) can be fitted to the points in Figure 5.

Available ^{13}CN lines, all from the violet system, are partially saturated, except for the $N'' = 3$ lines. Saturation means that the derived column densities depend on the b -value and the adopted splitting of the unresolved lines that make up the lines. In light of the fact that the b -values from CN and C_2 are in excellent agreement, we believe that the b -value is not a serious contributor of uncertainty to the determination of T_{rot} for ^{13}CN . Certainly, the column density of $N'' = 0$ cannot be lowered (relative to $N'' = 3$) by the 0.5 dex needed to make the ^{13}CN rotational temperature equal to that of CN.

From a study of millimeter emission lines (e.g., CO and CN) of seven planetary nebulae, Bachiller et al. (1997a) found a kinetic temperature of the CN line-forming region of only 25 K, and a rotational temperature of CN of 5–10 K. Quite unexpectedly, we found different rotational temperatures for CN and ^{13}CN of $T_{\text{rot}} = 11.5 \pm 0.6$ and $8.0 \pm 0.6 \text{ K}$, respectively.

In light of the continuing discrepancies between experimental and theoretical estimates for the CN red system f_R -values and the radiative lifetimes of the $A^2\Pi$ state, it is of interest to consider whether our spectra can give useful information on the ratio of the red- to violet-system f -values, f_R/f_V . Of course, the fundamental problem is that the strongest violet lines of a given N'' are much stronger than the strongest red-system lines of the same N'' (^{13}CN lines are of comparable strength to the red-system CN lines, but

the $^{12}\text{CN}/^{13}\text{CN}$ ratio is not independently known). A simple check of the f_R/f_V is possible by insisting that each band yield the same column density. We have conducted this exercise and found that relative to the violet system (0, 0) band, the red-system bands give a larger total column density by a factor of 2.3 (1–0), 2.4 (2–0), 2.1 (3–0), and 2.0 (4–0). To get consistent column densities, the f_R values must be increased by this factor. This is clearly unacceptable, and we will adopt our initial estimate of the f -values to proceed with our analysis. It seems that the correction factor is wavelength dependent: it increases with increasing wavelength. This could suggest that there is scattered light (continuum or CN line emission) that fills in the absorption profile. Since our observations are collected over several years (the red system was mainly observed in 1992 and the violet system only in 1997), there is the possibility that the strength of the lines has decreased with time. This idea can easily be tested by simultaneously observing both systems.

4.4. $\text{CN}/^{13}\text{CN}/^{14}\text{CN}/\text{C}^{15}\text{N}$ Isotope Ratios

Based on our findings of a different rotational temperature for CN and ^{13}CN , it is clear that the $\text{CN}/^{13}\text{CN}$ ratio will depend on the N'' levels included in the determination of the column densities. The $\text{CN}/^{13}\text{CN}$ ratio for each N'' level is given in Table 4, with an estimate of its uncertainty. In order to determine the isotope ratio of the line-forming region, we add the contributions from all N'' levels: $\text{CN}/^{13}\text{CN} = \sum_{N''=0}^5 N(N'')^{\text{CN}} / \sum_{N''=0}^3 N(N'')^{13\text{CN}} = 38.0 \pm 1.5$. If the measured T_{rot} is applicable to $N'' \geq 5$ levels, these bands contribute insignificantly to the summation.

Upper limits to the equivalent widths of 1.5 mÅ for both the ^{14}CN and C^{15}N lines correspond to lower limits of $\text{CN}/\text{C}^{15}\text{N}(N'' = 1) \geq 2000$ and $\text{CN}/^{14}\text{CN}(N'' = 1) \geq 2000$. Assuming that the rotational temperature of ^{14}CN and C^{15}N is equal to that of CN, we find lower limits of $\text{CN}/\text{C}^{15}\text{N} \geq 2000$ and $\text{CN}/^{14}\text{CN} \geq 2000$.

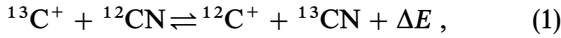
5. DISCUSSION

A Doppler parameter of $b = 0.51 \pm 0.04 \text{ km s}^{-1}$ sets an upper limit on the kinetic temperature of $T_{\text{kin}} = 400 \pm 50 \text{ K}$. This is rather high for gas that is about 10^{16} cm from the central star (Meixner et al. 1997). Based on radio observations of CN toward post-AGB stars, Bachiller et al. (1997a) argue that they find $T_{\text{kin}} \simeq 10\text{--}25 \text{ K}$. The b -parameter must, therefore, have an additional contribution from turbulence. The CN rotational temperature cannot be used to estimate the kinetic temperature, since the molecule is subthermal. C_2 behaves suprathermally, but the rotational temperature derived from the $J'' = 0$ and $J'' = 1$ level is a good indicator for the gas kinetic temperature. This would suggest $T_{\text{kin}} \simeq 189 \text{ K}$ (Bakker & Lambert 1997). This value is also much higher than expected, and it is clear that we need an independent accurate determination of the kinetic temperature. The turbulence required is in the range of $v_{\text{micro}} = 0.36\text{--}0.50 \text{ km s}^{-1}$ and depends on the adopted T_{kin} . The source of the turbulence is not identified, but it might be the result of small-scale turbulence, a non-Maxwellian velocity distribution, velocity stratification, or the presence of multiple unresolved absorption components produced by separate clumps.

An isotopic ratio as determined from molecules ($^iX^jY$ and $^jX^iY$) does not necessarily reflect the intrinsic isotopic ratio ($^iX/^jX$) of the gas. For example, interstellar (and probably circumstellar) CO is subject to two competing processes

that affect this ratio: photodissociation by line radiation and ion-molecule charge exchange (Watson, Anicich, & Huntress 1976). The net result depends on the local conditions (density, temperature, and radiation field).

Since photodissociation for the CO molecule is driven by line radiation, the more abundant the CO, the more the molecule can shield itself against dissociating by photons. The CN molecule is photodissociated by continuum radiation, not by lines. The ion-molecule reaction, on the other hand, will operate for CN. The gas-phase ion-molecule reaction for CN is given by



where ΔE is the zero-point energy difference derived from the molecular parameters (Prasad et al. 1992) and the relation of the isotopic dependence of the Dunham coefficients. We find 31, 58, and 23 K for ^{13}CN , ^{14}CN , and C^{15}N , respectively. The reaction to the right will be referred to as the forward reaction (k_f) and that to the left as the reverse reaction (k_r). C^+ can be produced by cosmic-ray ionization of free carbon atoms and molecules containing carbon (e.g., CO), and by the reactions of He^+ with these molecules (where CO is dominant).

Our picture of the chemistry of the CN molecule in the circumstellar shell is a simple one. CN molecules that are produced by photodissociation of the parent molecule HCN are subsequently destroyed by photodissociation. Between their formation and destruction, CN molecules participate in the isotopic exchange reaction. If the timescale for the isotopic exchange reaction is shorter than the lifetime of CN, then the exchange reaction will reach equilibrium:

$$R_{\text{eq}} = R_0/\alpha, \quad (2)$$

with

$$\alpha = \frac{k_f}{k_r} = e^{\Delta E/kT_{\text{kin}}} \quad (3)$$

$$R_0 = \frac{[^{12}\text{C}^+]}{[^{13}\text{C}^+]} = \frac{[^{12}\text{C}]}{[^{13}\text{C}]} \quad (4)$$

$$R_{\text{eq}} = \frac{[^{12}\text{CN}]}{[^{13}\text{CN}]}, \quad (5)$$

where square brackets denote the local density of that species in cm^{-3} , and R_{eq} and R_0 represent the equilibrium CN and true C isotope ratios, respectively. A lower limit to the kinetic temperature is given by the CN rotational temperature of 12 K. This gives an upper limit on α of 13. For higher temperatures, α decreases to unity. This clearly indicates that if the ion-molecule reaction is in equilibrium, we may underestimate the isotope ratio by as much as a factor 13. For a more realistic $T_{\text{kin}} \simeq 25$ K and an $R_{\text{eq}} = 23$, we find a true $R_0 = \text{C}/^{13}\text{C} = 80$.

To assess the behavior of the ratio $^{12}\text{CN}/^{13}\text{CN}$ in an expanding shell, we use the theoretical work of Cherchneff, Glassgold, & Mamon (1993) on the chemistry of the circumstellar shell surrounding the carbon star IRC +10216. The shell radius at which CN is more abundant than half its peak abundance is between 0.7×10^{17} and 1.3×10^{17} cm. Together with the expansion velocity, this gives a lifetime for CN of about 2×10^3 years. Basically, this is the lifetime of a single CN molecule after photodissociation of HCN, but before the photodestruction of CN, not taking into

account any other reaction that could produce or destroy CN.

The timescale for the ion-molecule reaction is more difficult to estimate. Adams, Smith, & Clary (1985) computed reaction rates (k_f) for polar molecules and found that they are as high as $10^{-7} \text{ cm}^3 \text{ s}^{-1}$ for low-temperature gas ($T_{\text{kin}} < 50$ K). The radius at which the CN abundance peaks ($r \simeq 1.0 \times 10^{17} \text{ cm}^{-3}$) has a C^+ abundance of $3 \times 10^{-4} \text{ cm}^{-3}$. The timescale for the isotopic exchange reaction, as derived from the forward rate coefficient and this C^+ particle density, is on the order of 1×10^3 years. The isotopic exchange reaction timescale is comparable to the CN lifetime. This suggests that we need to look into this process in some greater detail.

The effect of the isotopic exchange reaction should ideally be studied by computing self-consistent chemical models for the abundances and radiation field appropriate for HD 56126. Such a study is beyond the scope of this work; instead, we will make some estimates. A model of the circumstellar shell of the carbon star IRC +10216 has been computed by Cherchneff et al. (1993). This model uses a large number of chemical reactions, the interstellar radiation field, and circumstellar reddening to compute the abundances of the most important molecular species. The two major differences between IRC +10216 and HD 56126 are (1) the inner shell radius of HD 56126 will be much larger than for IRC +10216, and (2) the radiation field of HD 56126 (7000 K; Klochkova 1995) is significantly hotter than that of IRC +10216 (3500 K). The larger inner radius does not affect the chemical structure of the remaining shell. A 7000 K stellar radiation field has fewer UV photons than the interstellar UV field (see Paper II), so the interstellar radiation field will dominate the photodissociation processes. Therefore, the chemical structure of IRC +10216 is applicable to HD 56126. From the model, we infer that CN is produced mainly by photodissociation of HCN and destroyed by photodissociation into C and N. We take the CN and C^+ density (Fig. 6, *upper left*) from Cherchneff et al. (1993). Assuming that the isotopic exchange reaction for CN has reached equilibrium ($T_{\text{kin}} = 25$ K), we assume a true isotope ratio of $R_0 = 67$. From this we compute the source of the contribution to the observed column density (Fig. 6, *upper right*); the line is formed where the CN density is highest. For a range of reaction rates, we have computed the local CN and ^{13}CN densities, while the C^+ density is unaffected by the isotopic exchange reaction (Fig. 6, *lower left*). C^+ is mainly formed from CO, and the processes involved in the production of C^+ are not coupled to CN. The assumed reaction rate is $k_f = 1.0 \times 10^{-7}$. We see that the transition from the initial CN isotope ratio to the equilibrium value occurs where the CN density is highest and that this transition is rather fast. From these densities, we can compute the predicted observed CN isotope ratio (Fig. 6, *lower right*). To obtain an observed CN isotope ratio of 38 at $T_{\text{kin}} = 25$ K, we must start with an intrinsic isotope ratio of $R_0 = 67$ and $R_{\text{eq}} = 19$. Clearly, the isotopic exchange reaction is important. Based on this analysis, we suggest that the intrinsic carbon isotope ratio is $^{12}\text{C}/^{13}\text{C} = 67$ for $T_{\text{kin}} = 25$ K. Adams et al. (1985) show that the rate coefficient is dependent on the rotational quantum number. The higher the rotational quantum number, the lower the rate coefficient. If this dependence is rather strong, then the isotopic exchange reaction will be able to explain the difference in rotational temperature between CN and

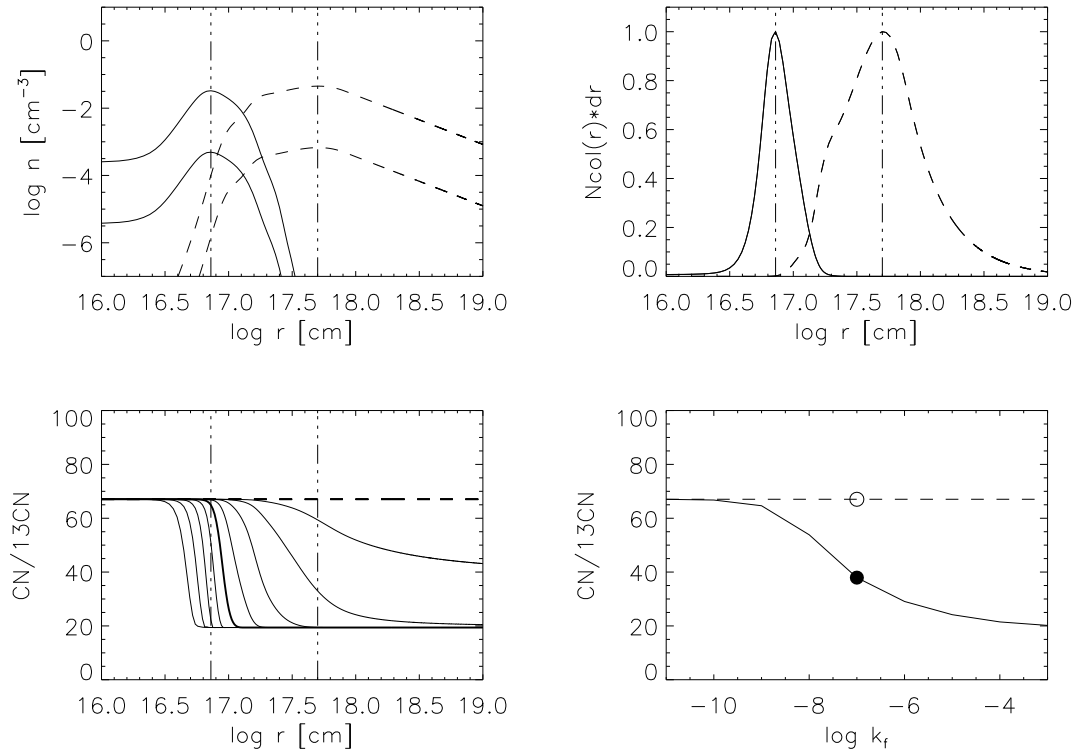


FIG. 6.—Upper left: Density of CN and ^{13}CN (solid lines) and C^+ and $^{13}\text{C}^+$ (dashed lines) as function of distance to the star (adopted from Cherchneff et al. 1993). Upper right: Contribution of the column density to the total column density, normalized to a peak value of 1. Lower left: Local isotope ratio for CN and C^+ as function of radius for reaction rates of $\log k_f = -11$ to -3 in steps of 1. The graph of $k_f = 1.0 \times 10^{-7}$ is enhanced. Lower right: Final observed isotope ratio, with a dot at our preferred rate coefficient.

^{13}CN : more ^{13}CN will be formed for $N'' = 0$ than for $N'' = 5$, leading to a lower CN isotope ratio derived from $N'' = 0$ than from $N'' = 4$.

Isotopic exchange reactions are very efficient at low temperatures and for high dipole moment molecules. From this we predict that CO (with a lower dipole moment) will be less affected, while C_2 , with no dipole moment, is unaffected. C_2 will therefore give the true isotope ratio, and combined with CN this may give the kinetic temperature of the gas. The isotopic exchange reaction also enhances the abundance of ^{14}CN and C^{15}N .

In order to derive the mass-loss rate from the CN absorption lines, we adopt the CN abundance (in number of particles) of $X_{\text{CN}} = 1.0 \times 10^{-6}$ for AFGL 2688 (Bachiller et al. 1997b). AFGL 2688 (the Egg Nebula) is so far the only C2CN group of stars for which radio emission of CN has been observed. The inner and outer radii of the ejecta of HD 56126 have been determined by Meixner et al. (1997) by modeling the spatial distribution of the infrared source: $r_{\text{inner}} = 45 \pm 2 \times 10^{15}$ cm ($1''.0 \pm 0''.15$) and $r_{\text{outer}} = 155 \pm 15 \times 10^{15}$ cm ($3''.6 \times 3''.3$ at $11.8 \mu\text{m}$). Assuming that CN coincides with the infrared source, we find $\dot{M} = 4.5 \pm 0.8 \times 10^{-5} M_{\odot} \text{yr}^{-1}$.

The prototype of the AGB stars, IRC +10216/CW Leo, is a massive, highly evolved carbon star with $3M_{\odot} \leq M_{\text{ZAMS}} \leq 5M_{\odot}$ (Guélin et al. 1995). For IRC +10216, the isotope ratios are well determined and give an estimate of the ratios that one might expect to detect for a carbon-rich post-AGB star such as HD 56126: $\text{C}/^{13}\text{C} = 44^{+3}_{-3}$, $^{12}\text{C}/^{14}\text{C} \geq 62600$, $\text{N}/^{15}\text{N} \geq 5300$, $\text{O}/^{17}\text{O} = 840^{+230}_{-170}$, and $\text{O}/^{18}\text{O} = 1260^{+315}_{-240}$ (see Forestini & Charbonnel 1997 for an overview). Our estimate of the $^{12}\text{C}/^{13}\text{C}$ ratio for the shell of

HD 56126 is consistent with that for IRC +10216. Results for circumstellar shells around four other carbon stars were provided by Kahane et al. (1992), who found $\text{C}/^{13}\text{C} \leq 60$, > 30 , 32^{+10}_{-7} , and 31^{+6}_{-5} . These also suggest that HD 56126 is not exceptional.

A comparison may also be made with isotopic ratios pertaining to the photosphere of cool carbon (AGB) stars. It must be borne in mind that the photospheric ratios may evolve before the stars shed the material that becomes the circumstellar shell of a post-AGB star. Luminous AGB stars of intermediate mass experience H-burning at the base of their convective envelopes. This decreases the $\text{C}/^{13}\text{C}$ ratio but also rather quickly converts the star from C-rich to O-rich. It seems improbable that C-rich post-AGB stars will have evolved from this intermediate stage. At lower luminosity and for lower mass stars, ^{12}C from the He-burning shell is added following a thermal pulse. Repetition of this addition will increase the photosphere's $\text{C}/^{13}\text{C}$ ratio unless H-burning converts ^{12}C to ^{13}C . In this scenario, the $\text{C}/^{13}\text{C}$ ratio of a post-AGB star might be higher than that of a typical AGB progenitor.

Through analysis of infrared spectra of N-type carbon stars, Lambert et al. (1986) showed that most stars had a $\text{C}/^{13}\text{C}$ ratio in the range of 30–70; a value of 67 is not unusual. Ohnaka & Tsuji (1996) reported systematically lower ratios from an analysis of spectra near 8000 \AA , but a ratio of 67 would not be unusual, although it would be on the high end of the distribution function. This possible shift between the $\text{C}/^{13}\text{C}$ ratio of stars and HD 56126 may be due to the fact that the stellar ratios continue to evolve before the post-AGB phase is reached. On the other hand, quantitative analysis of SiC circumstellar grains extracted from

meteorites shows a C/¹³C distribution function that mimics well the stellar distribution of Lambert et al. (1986), suggesting, perhaps, that evolutionary changes are minimal.

A priority goal must be the determination of more accurate C/¹³C ratios for HD 56126 and an adequate sample of post-AGB stars. In the case of HD 56126, the ratio is at present uncertain for several reasons. A minor contributor to the uncertainty is the combined use of CN violet- and red-system lines and the presence of uncertainty concerning the *f*-values of the red system. This uncertainty could be avoided by reobserving the strongest CN red-system bands at a higher S/N ratio, so that their ¹³CN lines are detectable. A key problem will remain that CN molecules are fractionated in the shell, which must be modeled in order to extract the C/¹³C ratio that is our primary interest. This extraction requires a better understanding of physical conditions in the shell. We suggest that this understanding might be obtained by analyzing spectra of other C-containing molecules. In particular, C₂ is accessible by the Phillips system, and CO is probably detectable in the infra-

red. Lacking an electric dipole moment, the isotopic exchange reaction involving C₂ will be very slow, and, as we have already shown observationally (Bakker & Lambert 1997), the C₂ and CN rotational ladders are influenced differently by the local density and the ambient radiation field. The CO molecule has a smaller dipole moment than CN, and its photodissociation is line dominated. Measurements of the ratios C₂/¹²C¹³C and CO/¹³CO, together with the CN/¹³CN ratio, will shed light on the physical conditions in the shell and on the true ¹²C/¹³C ratio. If such data can be assembled for a sample of post-AGB stars, it will be possible to trace a link with their AGB antecedents.

The authors acknowledge the support of the National Science Foundation (grant AST 96-18414) and the Robert A. Welch Foundation of Houston, Texas. We thank Joe Smreker for assistance at the telescope, and Eric Herbst for a discussion on the isotopic exchange reaction. This research has made use of the Simbad database, operated at CDS, Strasbourg, France, and the ADS service.

APPENDIX

HÖNL-LONDON FACTORS AND EFFECTIVE OSCILLATOR STRENGTH

Hönl-London factors were computed from the equations given in Schadee (1964) and Kovács (1969), and normalized according to the sum rule $\sum_{J'} S_{J'J''} = (2 - \delta_{0,\Lambda'+\Lambda''})(2S'' + 1)(2J + 1)$, as stated by (Larsson 1983). We take $S'' = 0.5$ for both the red and violet systems, since both originate from the same ground level (²Σ). For the red system (Π-Σ, $\Lambda' = 1$, and $\Lambda'' = 0$) we find $\delta_{0,1} = 0$, and for the violet system (Σ-Σ, $\Lambda' = 0$, and $\Lambda'' = 0$) we find $\delta_{0,0} = 0$. For the red system, we summed over 12 transitions following the selection rule, with $\Delta J = -1, 0$, and 1 , and $\Delta N = -2, -1, 0, 1$, and 2 ; six transitions for $N'' = J'' + 0.5$ and six for $N'' = J'' - 0.5$ for a given J'' ($P_1, Q_1, R_1, {}^Q P_{21}, {}^R Q_{21}, {}^P Q_{12}, {}^Q R_{12}, P_2, Q_2, R_2, {}^S R_{21}$, and ${}^O P_{12}$). For the violet system, we summed over six transitions following the selection rule, with $\Delta J = -1, 0$, and 1 , and $\Delta N = -1$ and 1 ; three transitions for $N'' = J'' + 0.5$ and three for $N'' = J'' - 0.5$ for a given J'' ($P_1, R_1, {}^Q P_{21}, {}^Q R_{12}, P_2$, and R_2). For both the red and the violet system this results in the relation $\sum_{J'} f_{J'J''} = 2f_{v'v''}$. The oscillator strengths of individual lines were checked against those of the SCAN tape (for the red system) and those listed in literature (for the violet system).

Given a Doppler broadening of $b = 0.51 \text{ km s}^{-1}$, transitions that are separated from each other by less than 0.012 \AA (violet system) and 0.022 \AA (red system) overlap, and the two transitions should be treated as one line with an effective oscillator strength. Lines that are separated by more than this interval should be treated separately, although they might not be resolved in the spectrum. In physical terminology, if lines are separated by less than the Doppler *b*-parameters, their optical depth at any frequency point should be added before computing the line profile [$I = e^{-(\tau_1 + \tau_2)}$]. If lines are separated by more than the Doppler *b*-parameter, the line profiles at any frequency point can be added ($I = 0.5e^{-\tau_1} + 0.5e^{-\tau_2}$), although adding the optical depth is also acceptable. For each blend, we can determine an effective oscillator strength in the following way.

The $F1$ ($J'' = N''0.5$) and $F2$ ($J'' = N'' - 0.5$) levels have different degeneracy:

$$g_e(F1) = 2J'' + 1 = 2N'' + 2 \quad (\text{A1})$$

$$g_e(F2) = 2J'' + 1 = 2N'' \quad (\text{A2})$$

Each N'' level therefore has a degeneracy of

$$g_e(F1 + F2) = 2(2N'' + 1) \quad (\text{A3})$$

This is even valid for $N'' = 0$, although that level has no $F2$ levels. The reason for this is that each J'' level is split into $2J'' + 1$ so-called *m* levels. Those levels are only separated from each other under the influence of a strong external magnetic field (Zeeman splitting). In the case of circumstellar CN, there is no observational evidence for assuming that these levels are separated, which indicates that there is no measurable magnetic field in the line-forming region. To first order, the *m* levels for $F1$ and $F2$ for a given N'' have the same energy and therefore the same population. This allows us to write

$$N(N'', F1) = g_e(F1)/g_e(F1 + F2)N(N'', F1 + F2) \quad (\text{A4})$$

$$N(N'', F2) = g_e(F2)/g_e(F1 + F2)N(N'', F1 + F2) \quad (\text{A5})$$

$$N(N'', F1 + F2) = N(N'', F1) + N(N'', F2) \quad (\text{A6})$$

$$f_{\text{eff}} N(N'') = \sum_i f_i N_i(N'') \quad (\text{A7})$$

$$f_{\text{eff}} N(N'') = \left[\sum_i f_i(F1)(N'' + 1) + \sum_i f_i(F2)N'' \right] \frac{N(N'')}{(2N'' + 1)} \quad (\text{A8})$$

As examples, we take two blends. For $\Delta N = N' - N'' = 0$ at 6194.5 Å (red system),

$$f_{\text{eff}} N(N'' = 1) = (0.091 \times 2 + 0.363 \times 1) \frac{N(N'' = 1)}{3}$$

$$= 0.182N(N'' = 1),$$

and for $\Delta N = N' - N'' = -1$ at 3876.3 Å (violet system),

$$f_{\text{eff}} N(N'' = 2) = (0.0132 \times 3 + 0.0022 \times 2 + 0.0110 \times 2) \frac{N(N'' = 2)}{5}$$

$$= 0.0132N(N'' = 2).$$

REFERENCES

- Adams, N. G., Smith, D., & Clary, D. C. 1985, *ApJ*, 296, L31
 Bachiller, R., Forveille, T., Huggings, P. J., & Cox, P. 1997a, *A&A* submitted
 Bachiller, R., Fuente, A., Bujarrabal, V., Colomer, F., Loup, C., Omont, A., & de Jong, T. 1997b, *A&A*, 319, 235
 Bakker, E. J., & Lambert, D. L. 1997, in *IAU Symp. 177, The Carbon Star Phenomenon*, ed. R. F. Wing, in press
 Bakker, E. J., van Dishoeck, E. F., Waters, L. B. F. M., & Schoenmaker, T. 1997, *A&A*, 323, 469 (Paper II)
 Bakker, E. J., Waters, L. B. F. M., Lamers, H. J. G. L. M., Trams, N. R., & van der Wolf, F. L. A. 1996, *A&A*, 310, 893 (Paper I)
 Bauschlicher, C. W., Jr., Langhoff, S. R., & Taylor, P. R. 1988, *ApJ*, 332, 531
 Bernath, P. F. 1995, *Spectra of Atoms and Molecules*, (New York: Oxford Univ. Press)
 Cherchneff, I., Glassgold, A. E., & Mamon, G. A. 1993, *ApJ*, 410, 188
 Davis, S. P., & Phillips, J. G. 1963, *The Red System ($A^2\Pi-X^2\Sigma^+$) of the CN Molecule* (Berkeley: Univ. California Press)
 Davis, S. P., Shortenhaus, D., Stark, G., Engleman, R., Jr., Phillips, J. G., & Hubbard, R. P. 1986, *ApJ*, 303, 892; errata *ApJ*, 307, 414
 Duric, N., Erman, P., & Larsson, M. 1978, *Phys. Scr.*, 18, 39
 Forestini, M., & Charbonnel, C. 1997, *A&AS*, 123, 241
 Gredel, R., van Dishoeck, E. F., & Black, J. H. 1991, *A&A*, 251, 625
 Guélin, M., Forestini, M., Valiron, P., Ziurys, L. M., Anderson, M. A., Cernicharo, J., & Kahane, C. 1995, *A&A*, 297, 183
 Hosinsky, G., Klyning, L., & Lindgren, B. 1981, *Rotational Analysis of the Red System $^{13}\text{C}^{14}\text{N}$. II. Wavenumbers, Term Values and Constants* (Rep. USIP 81-11) (Stockholm: Univ. Stockholm, Inst. Physics)
 Jackson, W. M. 1974, *J. Chem. Phys.*, 61, 4177
 Jenkins, F. A., & Wooldridge, D. E. 1938, *Phys. Rev.*, 53, 137
 Jørgensen, U. G., & Larsson, M. 1990, *A&A*, 238, 424
 Kahane, C., Cernicharo, J., Gomez-González, J., & Guélin, M. 1992, *A&A*, 256, 235
 Klochkova, V. G. 1995, *MNRAS*, 272, 710
 Knowles, P. J., Werner, H.-J., Hay, P. J., & Cartwright, D. C. 1988, *J. Chem. Phys.*, 89, 7334
 Kotlar, A. J., Field, R. W., & Steinfeld, J. I. 1980, *J. Mol. Spec.*, 80, 86
 Kovács, I. 1969, *Rotational Structure in the Spectra of Diatomic Molecules* (New York: American Elsevier)
 Lambert, D. L., Gustafsson, B., Eriksson, K., & Hinkle, K. H. 1986, *ApJS*, 62, 373
 Larsson, M. 1983, *A&A*, 128, 291
 ———. 1994, in *IAU Colloq. 146, Molecules in Stellar Environments*, ed. U. G. Jørgensen (Heidelberg: Springer), 271
 Larsson, M., Siegbahn, P. E. M., & Ågren, H. 1983, *ApJ*, 272, 369
 Lèbre, A., Mauron, N., Gillet, D., & Barthès, D. 1996, *A&A*, 310, 923
 Lu, R., Huang, Y., & Halpern, J. B. 1992, *ApJ*, 395, 710
 Luk, C. K., & Bersohn, R. 1973, *J. Chem. Phys.*, 58, 2153
 Meixner, M., Skinner, C. J., Graham, J. R., Keto, E., Jernigan, J. G., & Arens, J. F. 1997, *ApJ*, 482, 897
 Morton, D. C. 1991, *ApJS*, 77, 119
 Nyman, L. Å., Booth, R. S., Carlström, U., Habing, H. J., Heske, A., Sahai, R., Stark, R., Van der Veen, W. E. C. J., & Winnberg, A. 1992, *A&AS*, 93, 121
 Ohnaka, K., & Tsuji, T. 1996, *A&A*, 310, 933
 Oudmaijer, R. D., & Bakker, E. J. 1994, *MNRAS*, 271, 615
 Prasad, C. V. V., & Bernath, P. F. 1992, *J. Mol. Spectrosc.*, 156, 327
 Prasad, C. V. V., Bernath, P. F., Frum, C., & Engleman, R., Jr. 1992, *J. Mol. Spectrosc.*, 151, 459
 Schadee, A. 1964, *Bull. Astron. Inst. Netherlands*, 17, 311
 Tull, R. G., MacQueen, P. J., Sneden, C., & Lambert, D. L. 1995, *PASP*, 107, 251
 Utsumi, K. 1970, *PASJ*, 22, 93
 Watson, W. D., Anicich, V. G., & Huntress, W. T. J. 1976, *ApJ*, 205, L165